ELSEVIER

Contents lists available at ScienceDirect

Acta Biomaterialia

journal homepage: www.elsevier.com/locate/actbio



Full length article

Quantification of bush-cricket acoustic trachea mechanics using Atomic Force Microscopy nanoindentation



Eleftherios Siamantouras*, Charlie Woodrow, Emine Celiker¹, Darron A. Cullen, Claire E. Hills, Paul E. Squires, Fernando Montealegre-Z*

University of Lincoln, School of Life & Environmental Sciences, Joseph Banks Laboratories, Lincoln, LN6 7DL, United Kingdom

ARTICLE INFO

Article history: Received 15 April 2022 Revised 22 August 2022 Accepted 23 August 2022 Available online 30 August 2022

Keywords:
Outer ear
Respiratory trachea
Taenidia
AFM nanoindentation
Elasticity
Resilin
Finite element analysis

ABSTRACT

Derived from the respiratory tracheae, bush-crickets' acoustic tracheae (or ear canals) are hollow tubes evolved to transmit sounds from the external environment to the interior ear. Due to the location of the ears in the forelegs, the acoustic trachea serves as a structural element that can withstand large stresses during locomotion. In this study, we report a new Atomic Force Microscopy Force Spectroscopy (AFM-FS) approach to quantify the mechanics of taenidia in the bush-cricket Mecopoda elongata. Mechanical properties were examined over the longitudinal axis of hydrated taenidia, by indenting single fibres using precision hyperbolic tips. Analysis of the force-displacement (F-d) extension curves at low strains using the Hertzian contact model showed an Elastic modulus distribution between 13.9 MPa to 26.5 GPa, with a mean of 5.2 ± 7 GPa and median 1.03 GPa. Although chitin is the primary component of stiffness, variation of elasticity in the nanoscale suggests that resilin significantly affects the mechanical properties of single taenidia fibres (38% of total data). For indentations up to 400 nm, an intricate chitin-resilin response was observed, suggesting structural optimization between compliance and rigidity. Finite-element analysis on composite materials demonstrated that the Elastic modulus is sensitive to the percentage of resilin and chitin content, their location and structural configuration.

Based on our results, we propose that the distinct moduli of taenidia fibres indicate sophisticated evolution with elasticity playing a key role in optimization.

Statement of significance

In crickets and bush-crickets, the foreleg tracheae have evolved into acoustic canals, which transport sound to the ears located on the tibia of each leg. Tracheae are held open by spiral cuticular microfibres called taenidia, which are the primary elements of mechanical reinforcement. We developed an AFM-based method to indent individual taenidia at the nanometre level, to quantify local mechanical properties of the interior acoustic canal of the bush-cricket *Mecopoda elongata*, a model species in hearing research. Taenidia fibres were immobilized on a hard substrate and the indenter directly approached the epicuticle surface. This is the first characterization of the nano-structure of unfixed tracheal taenidia, and should pave the way for further *in vivo* mechanical investigations of auditory structures.

© 2022 The Authors. Published by Elsevier Ltd on behalf of Acta Materialia Inc. This is an open access article under the CC BY license (http://creativecommons.org/licenses/by/4.0/)

1. Introduction

Bush-crickets (Tettigoniidae; Orthoptera: also known as katydids) are a diverse group of insects that use sound for intra- and interspecific communication. Their ears, located in the proximal section of the foretibiae, each consist of two tympanal membranes per ear. These tympana are the outer ear component of the bush-cricket ear, transmitting sound through a middle ear system (the tympanic plate) to the inner ear (*crista acustica* or cochlea), following the same canonical steps as the mammalian hearing system [1]. Both tympana are backed by an air pipe derived from the respiratory system, the acoustic trachea (AT) or ear canal, which is also part of the outer ear [2–6]. The AT is a hollow, air-filled tube with the primary function of transmitting acoustic signals

^{*} Corresponding authors.

E-mail addresses: ESiamantouras@lincoln.ac.uk (E. Siamantouras), fmontealegrez@lincoln.ac.uk (F. Montealegre-Z).

¹ Current Address: University of Dundee, Division of Mathematics, Nethergate, Dundee, DD1 4HN, United Kingdom.

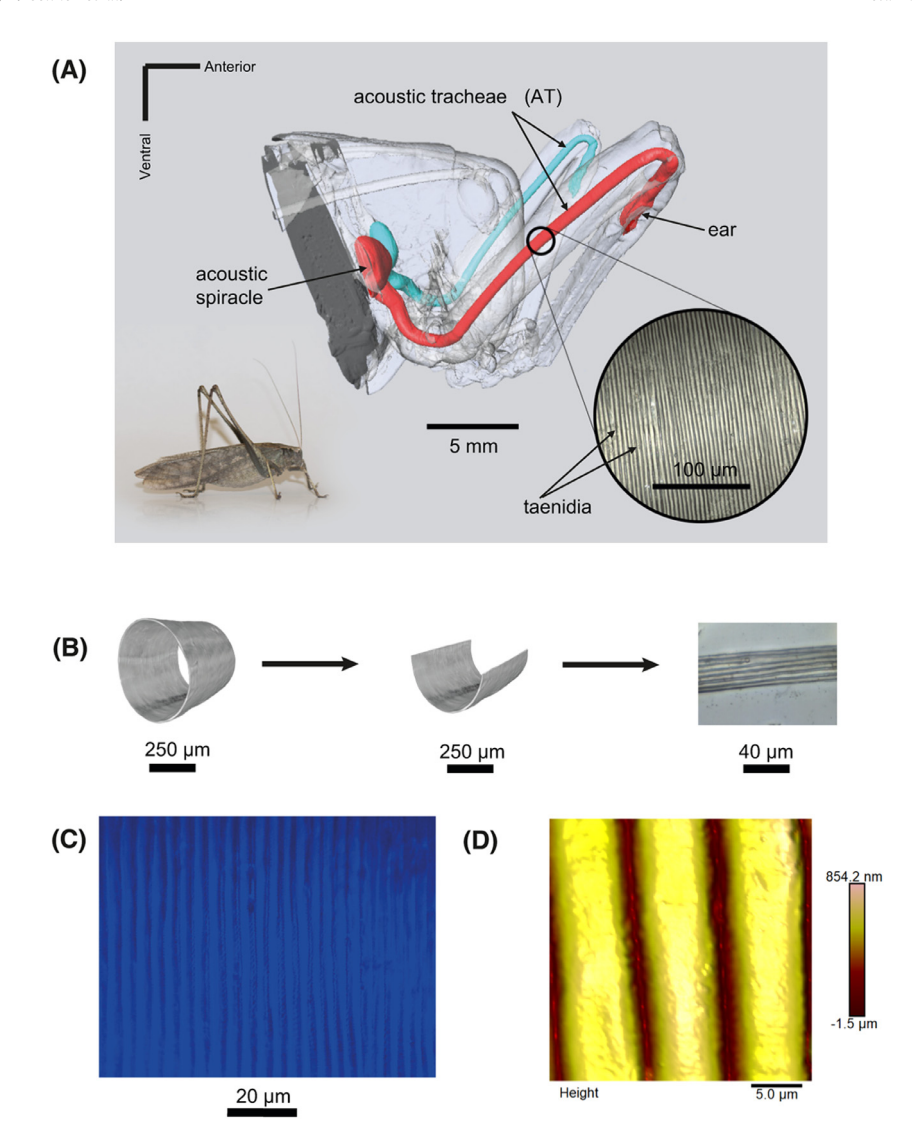


Fig. 1. Acoustic trachea of the bush-cricket *Mecopoda elongata*. (A) μ -CT 3D reconstruction of the tracheae. (B) μ -CT images of the trachea ex-situ, demonstrating the dissection technique and final microscopy image of a prepared strip of taenidia. (C) gross anatomy of the trachea under a light microscope, demonstrating UV autofluorescence under a DAPI filter set. Autofluorescence of the taenidia indicates the presence of resilin. (D) AFM topography image of the interior of the acoustic trachea showing flattened taenidia fibres attached on a PLL substrate.

from a spiracular opening on the side of the thorax to the internal surfaces of the tympana. The AT branches as it reaches the tympanic membranes, where the sound is received both internally from the AT, and externally through the air, with the dual effects of amplifying the sound and providing directionality, before reaching the auditory organ [7]. Due to its position throughout the leg of the animal, the AT has evolved to resist mechanical stress as it crosses through major leg articulations, between coxa and femur, and femur and tibia (Fig. 1A). On top of the trachea, between the two tympanic membranes, sit the inner auditory sensilla cells of the crista acustica, which highlights the key role of the AT in the structural support of the hearing configuration [8-10]. The AT must therefore be stiff enough to maintain shape and support in order to transmit vibrational signals to the cap cells of the crista acustica, but also compliant enough to allow quick recovery from movement/bending [11–13].

The multi-layered, inhomogeneous, complex micro-structure of the respiratory trachea poses significant challenges in its mechanical characterization [14,15]. The exterior surface is covered by epithelial cell layers responsible for the secretion of growth factors

[16]. Insect respiratory tracheae are formed by invaginations of the ectoderm, and thus lined by cuticular intima, continuous with the rest of the body cuticle [17,18]. The cuticle and other materials form a meshwork of fibres with multiple organization separating the epithelium from the inner side. In its interior, the structure becomes more definite, with taenidia organized circumferentially creating a fibre-composite tube, with a layer of resilin beneath the epicuticle [19]. Taenidia are formed as differentiated thickenings of the cuticular intima [18]. Characterization of their fundamental deformation behavior can lead to better understanding of the structural reinforcement of the trachea.

Similar to the respiratory trachea, the AT is a composite tube that is covered by a continuous sheet of soft epithelial cells, and complex chitinous cuticle sublayers [20]. The chitin-based multilayer micro-structure develops mostly in the inner section of the tube [12,21]. The inhomogeneity of the composite tracheal tubes determined by the intricate arrangement of its components [22], poses an additional challenge to the evaluation of their mechanical properties. The taenidium, which develops along the inner side of the tube, is the main structural element of all in-

sect tracheae and enables the AT to function under mechanical loading [12]. Although mostly made of chitin-based cuticle material, trachea gains its mechanical resilience from an elastomeric protein, resilin that is found in numerous insects [23–25]. Therefore, the acoustic trachea maintains its ability to withstand loads with the aid of a composite structure, that is mainly made of tightly coiled, chitin-elastin fibres uniformly organized as a spring in the inner trachea where sound travels [18]. The two-fold biological function of an acoustic trachea as both a sound transmitting tube and structural support depends largely on its mechanical properties [26].

Taenidial thickenings are the basic supporting elements of the interior tracheal wall and the primary source of trachea reinforcement in insects [17], and this has been well documented in the American cockroach, Periplaneta americana [27]. In addition, Webster et al. [12] suggested that branching and fusion of taenidia confer a circumferentially non-homogeneous Elastic (Young's) modulus that was also related to the collapse of the trachea, in addition to the cross-sectional shape. Although taenidia present a considerable level of uniformity in their organization, there are branches that are developed in bifurcations for a few microns before fusing into a single fibre. Branching and fusion may cause discrepancies in bulk methods. Macroscopic methods of characterization, such as whole tube compression may detect bifurcations as heterogeneities of the microscopic structure. Apart from the difficulties accessing the taenidia from the exterior of the tube, such complex material is considered anisotropic hence the modulus will be direction dependent [28]. Tracheae used for acoustic transmission may have evolved differently due to the differences in the transmission of media (e.g. sound waves optimization), nevertheless the principle of AT architecture is still the same. Determining the Elastic modulus of single taenidium fibres can help the numerical analysis of 3D mechanical loading, 3D acoustic models and the development of better models relating material defects with deformation or failure of cylindrical structures.

Here, we report a new Atomic Force Microscopy (AFM)-based experimental approach to characterize local mechanical properties of taenidia by nanoindentation. Our experimental study assesses the contact mechanics of a taenidium fibre and can elucidate its elastic properties for a better understanding of the mechanics of the interior tracheal tubes. We describe a method by which the sample does not require drying, extensive chemical or other structure-altering manipulation. It can be applied to fresh trachea samples and allows maintenance in saline during mechanical testing. AFM is a powerful tool for high-resolution force measurements and AFM nanoindentation is a well-established technique for the investigation of mechanical properties of biological materials [11,29]. We have considered each taenidium thickening as a single fibre, and we quantitatively investigated its elastic properties. By using the AFM as a force spectroscopy tool and by employing a cantilever with a fine tip, nanoscale mechanics were examined. The molecular structure of the material was probed by a fine indenter, while the resistance was detected by the deflection of a sensitive cantilever. Fresh, unfixed taenidia fibres were used for nanoindentation experiments extracted from the AT of Mecopoda elongata, a model species for hearing research. Accurate characterization of the AT inner wall mechanics can provide interdisciplinary insights into acoustic transmission, potential passive amplification characteristics, and frequency tuning. As a validation of the empirical results obtained and to go beyond experimental limitations, a finite element analysis of the problem was also carried out. Such a complementary study is necessary to provide a fundamental understanding of the mechanics governing the basic structural element in specialized acoustic tracheae of insects and form the basis for advances in smart bio-inspired, biomedical applications.

2. Methods

2.1. Sample preparation

Adult specimens of Mecopoda elongata were obtained from colonies reared at the University of Lincoln. Specimens were housed in a shared enclosure at a mean temperature of 25 °C and were maintained on an ad libitum diet of bee pollen (Sevenhills, Wakefield, West Yorkshire, UK), fresh apple, and dog food, with access to water. Individuals were anesthetized using a mild ethyl chloride spray (Chemische Fabrik Walldorf GmbH, Walldorf, Germany) prior to removal of the forelegs, and were returned to the colony once awake. The whole foreleg was immersed in 0.9% saline solution (0.9 g sodium chloride per 100 mL) and pinned at the proximal and distal ends of the forefemur using 40 mm steel pins (Austerlitz, Czech Republic). The cuticle of the forefemur was dissected under a microscope using micro spring scissors (Vanaas scissors, World Precision Instruments, Friedberg, Germany) to expose the acoustic trachea. The acoustic trachea tube was cut at both ends, extracted with micro tweezers, washed in saline, and was partially bisected longitudinally using the micro-scissors. This part of the tube is uniform in diameter and was used for further manipulation. Microsamples consisting of multiple taenidia were isolated from the open tube using micro-scissors, forceps and fine tweezers and washed with saline or sterile water. Any excessive material that would obstruct mechanical testing was removed at this stage. These tracheae samples, typically containing 10-20 taenidial fibres, were transferred into a dry 35 mm Petri dish [TPP Tissue Culture dish, Sigma-Aldrich, UK). With the aid of the microscope, a small portion of glue (Gorilla J0012 Epoxy Glue), was applied to the sides to ensure stability of the sample and avoid any bulging due to media buoyance. The width of the sample was larger than 50 microns. Saline was added to the immobilized sample within 2 min. Samples not properly adhered would float on the edges and several attempts may be necessary to achieve media insulation. Although sample preparation may have taken up to 2 h per sample, mechanical properties will not suffer from chemical modification and the sample did not dehydrate. Fresh samples were maintained in saline at room temperature during experiments and tested within 2 h of extraction.

Fig. 1A and B shows the AT of the bush-cricket Mecopoda elongata. The X-ray µ-CT settings and three-dimensional (3D) reconstruction software are based on procedures described in Veitch et al., Jonsson et al., and Celiker et al. [7,30,31], using a Bruker Skyscan. For AFM and scanning electron microscopy (SEM) imaging animals that were stored in the freezer (-20 °C) were used. The legs of the animals were thawed from preservation and the dissection procedure was followed. The taenidia sample was then immobilized on a Petri dish coated with 0.01% poly-L-lysine (PLL) (P4707; Sigma-Aldrich, UK). Coating of the dish substrate was achieved by fully covering the surface of the dish with 2 mL of PLL for 5 min at RT, then removing the media and incubating the dish at 55 °C for 30 min. After repeating this process three times per dish, the PLL coated substrate was washed with sterile water and the plates were stored at 4 °C. The thawed trachea was transferred to the PLL dish in saline and gently submerged until it adhered to the substrate. Spring scissors were inserted at one end to cut along and open up the trachea. The immobilized sample was washed twice with sterile water.

2.2. Resilin fluorescence microscopy

Fresh acoustic tracheae were imaged on a compound microscope (Olympus BX51WI, Olympus, London, UK) under both bright field and UV illumination. UV light was conditioned by a DAPI filter set (DAPI-5060B Brightline series, Semrock, Rochester, NY, USA)

with a sharp-edged transmission band from 350 to 407 nm. The resulting blue fluorescence emitted from the AT sample was collected in a similarly sharp-edged band at blue wavelengths from 413 to 483 nm through a dichroic beam splitter. Images were taken using a Micropublisher 5.0 digital camera (Q Imaging, Marlow, Bucks, UK).

2.3. AFM imaging

Imaging was conducted in fluid using the Bruker AFM (Bruker Nano Surfaces & Metrology, Santa Barbara, CA) in combination with an inverted microscope (Nikon TE-2000S, USA). The sample was immobilized on a PLL-coated Petri dish. Scanning was performed using triangular ScanAsyst-Fluid+ cantilevers (nominal spring constant: 0.7N/m, Tip radius: 12nm) in saline at room temperature. Imaging was performed in constant force mode where the piezo's Z height is controlled by a feedback loop to keep the deflection of the cantilever constant. The loading force is related proportionally to the deflection of the cantilever via the spring constant. Imaging parameters such as setpoint, gain and scan rate were optimized by using Peak Force Tapping mode under ScanAsyst adaptive settings. Scanning was performed at a low rate of 0.1 Hz for capturing strips of taenidia fibres (maximum size scanned: 26 µm) with a sampling resolution of 128 points per line and peak force set point between 40 and 60 nN. At least 10 different areas were scanned from different samples (N = 2) and the representative Peak Force Tapping (PFT) height images were flattened (order 1).

2.4. SEM imaging

The acoustic trachea was partially bisected longitudinally to reveal the interior side and fixed in a solution of 2.5% glutaraldehyde in 0.01 M phosphate-buffered saline (PBS) for 30 min. The extracted taenidia samples were washed in PBS and double-distilled water (ddH₂O) for 10 min, respectively. The samples were then dehydrated in an ethanol series (10 min each in 30%, 50%, 70%, 90%, 100% x2) and dried inside microporous specimen capsules (Agar Scientific) in a critical point dryer using CO₂ (Quorum E3100). Three samples were attached to aluminium SEM stubs using double-sided carbon tape and coated with 15 nm iridium using a sputter coater (Quorum K575X). Samples were viewed using a Verios 460 SEM (ThermoFisher/FEI) operated at an accelerating voltage of 2 keV and a 25 pA probe current. Low magnification images were taken using an ETD detector at long working distance, while higher resolution images were taken using the TLD detector in immersion mode at a working distance of around 3.4 mm. Intact areas (3 samples of 1 acoustic trachea) were used to analyze the micro-nano-scale architecture of single taenidia fibres, crosssection and interior surface. The images were obtained in areas that were free from any obvious damage during sample prepara-

2.5. AFM nano-indentation

Elastic (Young's) modulus is an elastic property of a material under deformation, defined as the ratio of stress to strain. In AFM nanoindentation, the surface of the material is locally indented with an indentation geometry that is tip shape dependent. The Hertz model describes the contact mechanics of two spheres under a shallow indentation and is a broadly used model to analyse AFM force-displacement curves. The model describes the elastic deformation of two perfectly homogeneous smooth bodies that are brought in contact under load. Although, the original Hertz model normally fits a circular paraboloid indenter, Hertzian contact mechanics also refers to a number of associated models that

have been modified based on the indentation geometries and the radius of contact [32]. The determination of the Elastic modulus was performed using the Sneddon's variation for purely elastic indentation by a stiff cone tip [33,34]. The relationship between the applied loading force F and the indentation depth δ of the tip can be described as follows,

$$F = \frac{E_s}{\left(1 - \nu_s^2\right)} \frac{2 \tan a}{\pi} \delta^2 \tag{1}$$

where E is the Elastic modulus (the most generic term will be used), ν is the Poisson ratios of the sample and a the half-cone opening angle of the AFM tip.

In AFM indentation the vertical deflection of the cantilever is continuously measured as a function of the piezo-actuator height, in order to produce force-indentation curves. Briefly, the actuator moves the base of the cantilever downwards in the vertical direction until a preset force is achieved after which the cantilever is retracted (Fig. 2A). The loading force F was calculated from the product of the cantilever vertical deflection and the spring constant k of the cantilever (calibrated before each experiment). Initially the vertical deflection of the cantilever is measured as a function of the piezo-actuator height. However, the position of the actuator after the contact point, does not always correspond to the indentation depth of the sample. Bending of the cantilever against the sample in the opposite direction of indentation, can induce an error in the displacement axis of the experimental measurements $\delta_{\rm deflection} = \delta_{\rm bending} + \delta_{\rm indentation}$ [35].

There are specific assumptions about the sample using Hertz model and considerations must be made for its validity [36]. Since the indenter tip radius (10 nm) was much smaller than an approximation of the radius of the sample (7 µm), we assumed that the tip loading is applied to a semi-infinite, elastic half-space. Fig. 2B shows an optical microscopy image of an AFM nanoindentation experiment. Force-displacement measurements were taken near the centre of the taenidia fibre. To satisfy all Hertzian assumptions, the sample was considered to be homogeneous, isotropic and linear. Elastic modulus was determined by analysing the extension part of the curve that is free from adhesion effects. In order for the elasticity assumption to be valid, all indentations were performed at less of 5-10% of sample thickness [33]. Stress can be considered proportional to strain under small deformations and can be characterized by a linear elastic model. Indentation at 5-10% of the sample's height ensures that substrate effects were negligible during the experiments. The contact point was defined as the intersection point between the corrected slope in cantilever deflection and the horizontal axis that represent the non-deflected plane. Overall, the exact contact point that designates the point where the tip first touches the surface is difficult to be established and approximations were used [42].

2.6. Experimental instrumentation

Force-displacement curves in vertical indentation were obtained using the CellHesion®200 AFM module (JPK Instruments, Berlin, Germany) that was installed on an Eclipse TE 300 inverted microscope (Nikon, USA). Temperature during experiments was monitored by incorporating the BioCellTM controller (JPK Instruments, Germany) into the AFM stage. The temperature was maintained at 21 °C throughout experiments, while changes in the room temperature were less that 0.5-1 °C. Manipulation of the sample and phase microscopy images were acquired using a CCD camera (Orca, Hamamatsu, Japan) connected to the side port of the microscope. The AFM set-up was driven by JPK's CellHesion200 software. The entire recording instrumentation was supported on an antivibration table (TMC 63-530, USA). Rectangular cantilevers with sharp hyperbolic tips (QP-fast nominal force constant 15, 30, 80

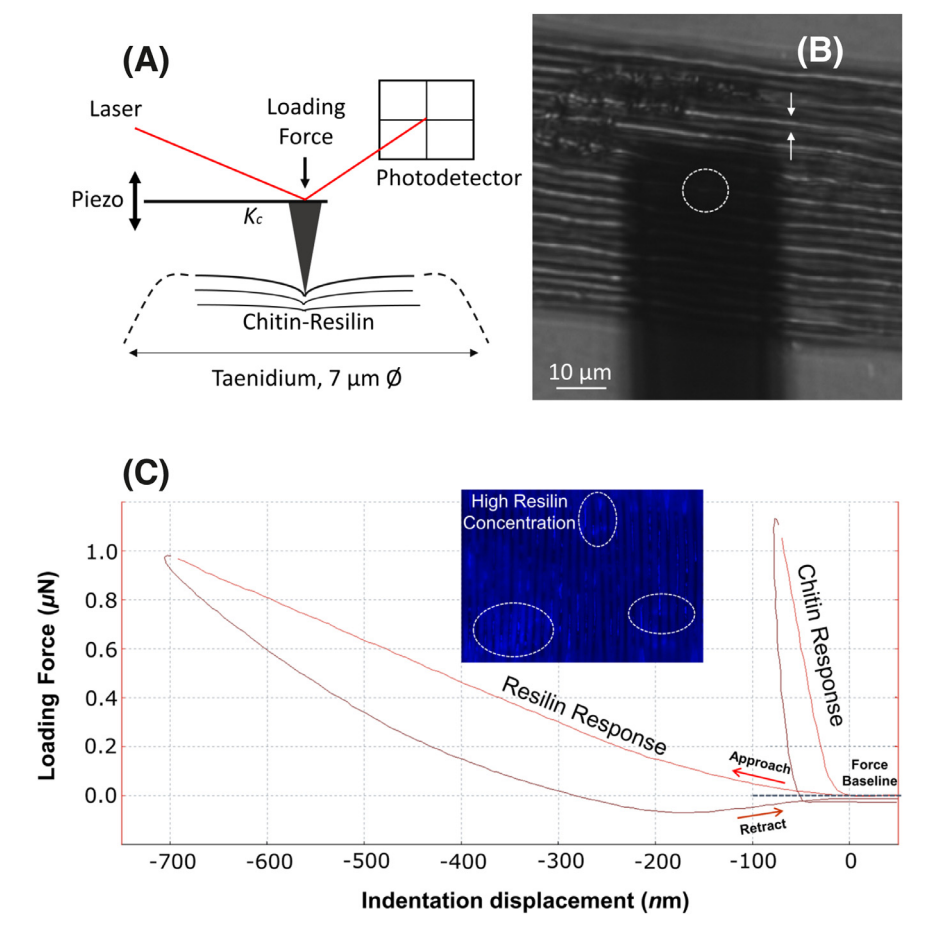


Fig. 2. AFM Nano-indentation approach. (A) Basic components of AFM and sample (not to scale). The cantilever is stationary in x-y direction, while the z position is controlled by a piezo motor. The laser reflects on the photodetector the deflection of the probe. Mechanical contact is controlled via feedback between the piezo and the photodiode. Using spring stiffness, the applied force is calculated by multiplying the calibrated spring constant with the deflection of the cantilever ($F = K_C \times d$). (B) A rectangular cantilever at the retracted position, 100 µm from surface. Focus is on the substrate sample, the centre of the dotted circle shows the top view of the indenter. (C) Distinct force-displacement response at different local indentation points under a loading force of 1 µN in the central region of taenidia. Discrete regions marked with a white circle demonstrate differences in autofluorescence intensity, that were detected by significant variations in Elastic modulus.

N/m, Ø 10 nm NanosensorsTM uniqprobe, Switzerland) were used to indent the material. Deflection of the cantilever was measured by the reflection of the laser beam onto a quadric-sected photodiode (Fig. 2A). The cantilever was calibrated prior force recordings to determine the actual spring constant value, using the manufacturer's software (JPK Instruments, Germany) using the Sader method for rectangular cantilevers [35,37,38]. The AFM tip was approached and indented the surface at a constant velocity of 3 μm/s. The sample was attached in substrates in Petri dishes and was maintained in saline during experiments (0.9%) at 21 °C. Three successive force-displacement curves with 45 s relaxation intervals were performed at central regions away from the taenidium boundary (Fig. 2B). The tip shape is circular symmetric with a hyperbolic profile, a small tip radius < 10 nm and a typical tip height of about 7 mm. Due to the hyperbolic tip shape the macroscopic cone angle is a function of the distance from its apex. In the first 200 nm of the tip apex the half cone angles are comprised between 12° and 18°.

2.7. Numerical simulations

The structural mechanics Module of Comsol Multiphysics v. 5.6 was used for the simulation of the nano-indentation process on an idealized taenidium fibre [Comsol v. 5.6]. In accordance with the experimental procedure, the nano-indenter was taken to be a cone of height 5.93 µm, tip radius 10 nm and half-cone angle 12°. The

idealized taenidium was modelled as a cylinder, with a radius 2.5 μ m and length 100 μ m (Fig. S1 in supplementary material demonstrates the geometry used in the model). The material of the indenter was assumed to be isotropic and homogeneous, with an Elastic modulus of 200 GPa, Poisson's ratio 0.3, and density 8000 kg/m³.

During the simulations, we used the fixed values of 0.3 for Poisson's ratio and 1000 kg/m³ for density to define the taenidia fibres. Further, the taenidia material was considered to be isotropic, with simulations considering both homogeneous and heterogeneous properties. For the validation of the model, we assumed the material to be (i) pure resilin (Elastic modulus 32 MPa), and (ii) pure chitin (Elastic modulus 2 GPa). Hence, Elastic modulus was set-up as an independent variable. The obtained results were used to directly compare with the experimental data. With the validation of the model, we also considered the Elastic modulus of the taenidia fibre when it was comprised of a combination of pure resilin and pure chitin. These compositions were

- (a) the top half of the taenidia resilin and the botton half chitin;
- (b) the left half of the taenidia resilin and the right half chitin;
- (c) a random variation of resilin and chitin along the surface of taenidia, with a resilin (top half) and chitin (bottom half) split within the fibre;
- (d) horizontal strands of resilin and chitin with a smooth transition between the strands.

The heterogeneous materials considered are graphically represented in Fig. 8. In this case, the overall Elastic modulus was considered a dependent variable, and the Hertz-Sneddon model given in Eq. (1) was applied for calculating the Elastic modulus from the force-displacement curves obtained through the simulations.

To make the simulation of the model computationally feasible, the initial mesh size was prescribed to be a relatively coarse mesh for both the taenidia and the indenter (a tetrahedral mesh of maximum element diameter 2 μm and minimum element diameter 0.001 μm). The regions requiring higher resolution were then identified through adaptive mesh refinement [39]. The mesh size would be reduced based on the residual error calculated in the functional norm, which was applied to the global vertical displacement. The final form of the mesh can be seen in supplementary material, Fig. S1. Due to the shallow indentation depth, a linear system of equations was considered for the solution, hence the linear elastic material node of the Solid mechanics module [40] was employed to model the taenidium fibre. In accordance with the experimental set-up, the bottom of the taenidium fibre was fixed, while the rest did not have any constraints.

The contact problem was solved by the augmented Lagrangian method, where a zero initial gap was assumed without any forces between the indenter and the fibre. The contact pair was set-up through a definition for the master and slave bodies, where the indenter was defined as a master and the taenidium as a slave. The contact model was adapted to reflect the quadratic relationship between the indentation depth and force as given in Eq. (1). The model was implemented in indentation control mode, hence for the homogeneous material models the force magnitude was calculated through the model for a prescribed Elastic modulus and indentation depth. The indentation depth was applied through a prescribed vertical displacement of the indenter, where the indentation depth was taken based on the experimental data. The vertical indentation was applied with a continuation from the last parameter. Finally, orce-displacement graphs were obtained from the results of the simulations . A similar process was also applied for the heterogeneous material models, with an additional step of calculating the composition Elastic modulus from the obtained forcedisplacement curves. The described models were solved as a stationary study, from which the vertical reaction force was obtained on the surface of the taenidium fibre that was in contact with the indenter.

2.7. Data processing

All F-d recording were processed and analysed using commercial data processing software (JPK Data Processing Version spm-, JPK Instruments, Germany). AFM image processing was done using the NanoScope Analysis 1.9 (Bruker Nanosurfaces, USA). SEM section measurements were conducted using ImageJ (Java 1.8.0_172 open-source Imaging Software). Statistical analysis was performed using SPSS (IBM Statistics, version 24). Data from SCFS are expressed as mean \pm SEM in the text and as median and interquartile range in the figures. To signify statistical differences data were evaluated using the independent samples t-test.

3. Results

3.1. Morphology and size of taenidia fibres

Microscale topography using AFM showed the surface morphology and architecture of the taenidia (Fig. 3A-C). The dimensions and shape of taenidia were estimated from AFM height images. The 2D height image of three taenidia fibres is shown in Fig. 3A. Cross section analysis was used to calculate the width and height

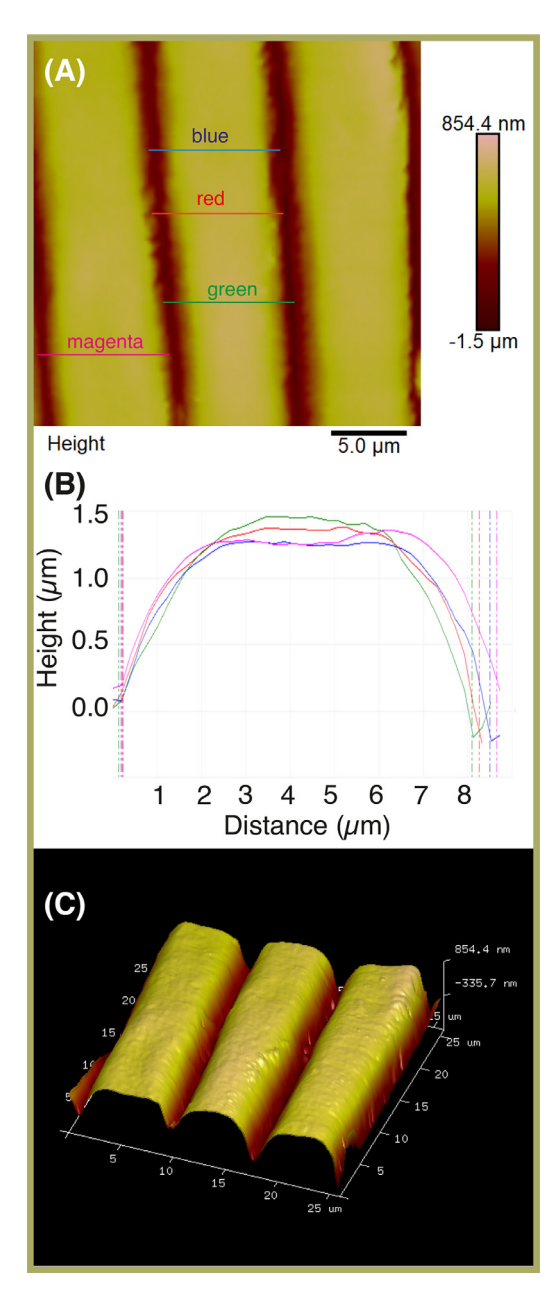


Fig. 3. AFM topography imaging showing the architecture of taenidia attached flat in a PLL substrate. (A) Peak Force Tapping (PFT)/ScanAsyst image of 2D taenidia fibres (BioScope Catalyst) in saline , using ScanAsyst Fluid+ AFM probes (k: 0.7N/m). Scan area: 26 μ m, rate: 0.1Hz, set point 250mV. (B) Cross section of taenidia, as indicated by the lines, showing the width and height of fibres from the bottom point between the thickenings. (C) 3D PFT image of a taenidia microstrip scan (26 \times 26 μ m), showing the architectural configuration of the interior acoustic trachea.

of the thickening in relation to the gap. The base reference to determine the height and boundaries of the thickening is shown in Fig. 3B. The measured mean size of five cross-sections in seven fibres for height and width distance was $2.3\pm0.2~\mu m$ and $7.6\pm0.3~\mu m$ respectively. The height of taenidia from the bottom of the cuticle thickening was used to inform the 5-10% least rule of indentation depth during experiments and modelling. In addition, AFM topography showed that the thickening of the taenidia is developed as a relatively flat surface in the central region. From the 3D profile of the taenidia, it can be observed that the topography of the thickening of the fibres is identical (Fig. 3C). Electron microscopy cross-section measurements of the central distance between the outer surface and the boundaries between the taenidia main body

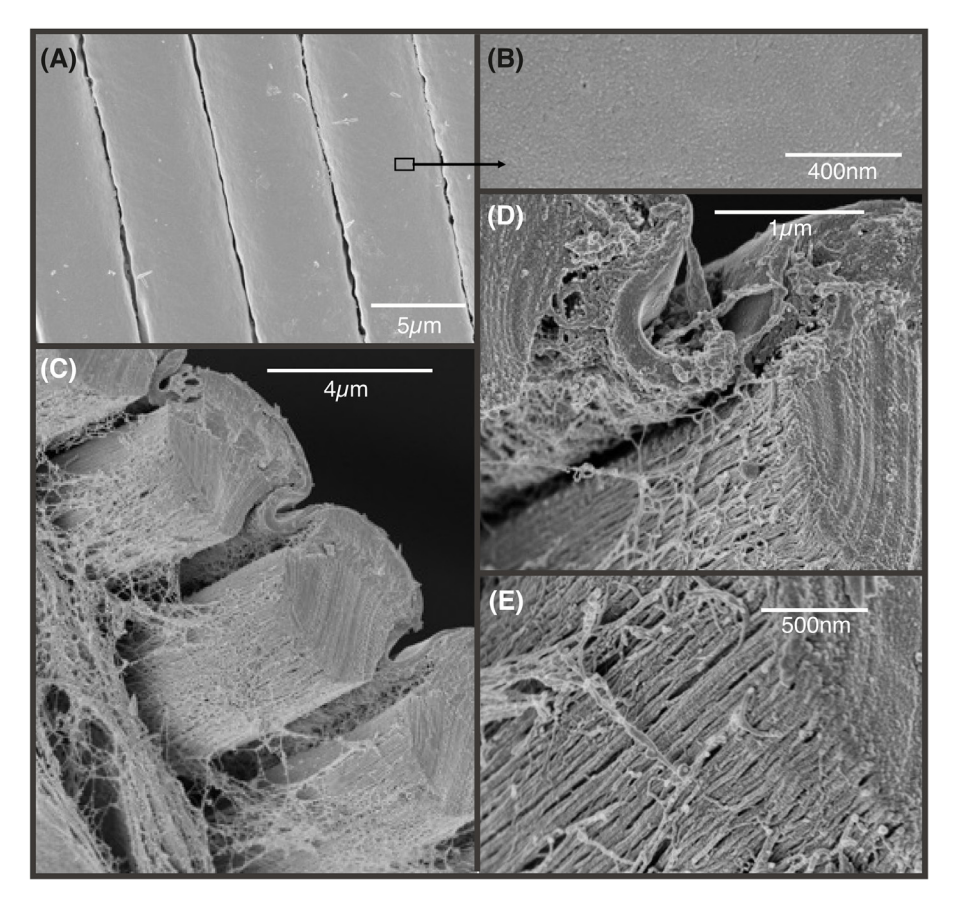


Fig. 4. SEM imaging of taenidia fibres. (A, B) Top view of taenidia showing uniformity of the thickening development and exterior surface. (C) Perspective of taenidia fibre where the epithelial sheet and mesh network was peeled showing the interior body of the fibre. (D, E) Structural organisation of the nanofibrils comprising the main body of the taenidium and outer surface layer.

and loose mesh, showed mean height 3.8 \pm 0.3 μ m (6 taenidia). This value is within the range of the assumption for mechanical analysis using the Hertz model. Fig. 4 shows SEM images of the taenidia surface (A, B), cross section and angle perspective (C, D, E). Specifically, in areas where the loose mesh of chitinous material was peeled the structure of the material underneath, revealed the interior configuration of the taenidium. Measurements of the width of single nanofibrils that were attached in the main body of the fibre with no obvious damage, were estimated at 18 \pm 5.5 nm (19 nanofibrils).

3.2. Force-displacement response

AFM force-displacement curves provide important information about the mechanical response of the sample. As the cantilever moves downwards to approach the sample, F-d curves show a clear region, where there is no force between the tip and the surface, which is defined as the force baseline and can be used to estimate the contact point. After contact, the loading force generates a certain indentation displacement which is associated with the deformation of a material, i.e. soft materials show higher indentation depth under a specific force set-point. Fig. 2C shows forcedisplacement curves that corresponded to distinct mechanical responses at different local indentation points under a loading force of 1 µN in the central region of taenidia. In resilin-response area the force produced an indentation depth of 700 nm and an Elastic modulus of 20.4 \pm 1.5 MPa, compared with 70 nm and 2.5 \pm 0.3 GPa in the chitin-response area. Elastic response is a characteristic of the soft, rubbery protein resilin [41] and UV microscopy confirmed that taenidial fibres exhibit a bright blue autofluorescence in the DAPI range (Fig. 1C, Fig. 2C). The retraction process of compliant F-d curves showed adhesion forces before complete separation, while the F-d response of the rigid points indicated elastic-plastic deformation.

Indentation was controlled by the force settings rather than displacement as in z-height indentation. The contact point was in the region of contact between the force baseline and the y-axis and the exact value was difficult to define. It was detected by identifying a positive ramp on the force baseline axis and a displacement window (10-15 nm) was used to approximate the contact point. after which the curve was entering a linear phase [42]. There was substantial variation in the indentation depth produced by loading forces, which was dependent on the composition of chitin-resilin in the local area of the taenidium. Since different local points showed significant differences in mechanical response, force and indentation depth were assessed between indentation points. For compliant points, the forces and corresponding indentation depths were between 30-1000 nN and 55-330 μm, whereas for stiff points were between 110-850 nN and 30-90 μm (The relationship between force and indentation depth can be found in supplementary materials, Fig. S2). The force indentation method has the advantage of faster experimental procedure, provided that the 5-10% rule is consistently maintained. However, the experiment required a broad range of loading forces to optimise indentation depth based on the local response of the material. As a precaution, the curves were fitted to various incremental indentation depths to monitor for any large differences in Elastic modulus, that may be induced due to substrate effects or changes in material composition.

3.3. Mechanics of individual taenidia

The loading part of the F-d curve, which was free from adhesion, was analysed to compare the Elastic moduli of different local indentation points. The modified Hertzian/Sneddon contact model for conical tip was applied to the constant compliance region up to 300 nm. For indents larger than 10-20 nm and less than 200-300 nm, the cone describes accurately the profile of the tip. At this range the half-angle fitting parameter was kept constant at 12° for all indentation curves. Poisson ratio was set at 0.3 and was kept constant for both variables. The local elastic modulus of taenidia fibres indented centrally by a fine tip with radius of curvature smaller than 10nm, was found to be in the range between 13.9 MPa to 26.5 GPa (mean = 5.2 ± 7 GPa, median = 1.03 GPa, N of trachea = 3, local indentation points = 28).

Analysis of the Elastic modulus in relation to forces showed distinct variation between the mechanical response of the chitinresilin composite taenidia (Fig. 4A). Forces higher than 150 nN created a gap in material response that was increased further with higher forces. However, the lower range of Elastic modulus comprised 38% of the total data set (Fig. 4B). This distribution demonstrates that resilin may had a key role in the evolutionary optimisation of the fibre-composite tube and the functional reinforcement-recovery adaptation. The pronounced differences in the material response between chitin and resilin resulted in statistical significance of Elastic moduli, P<0.001 (Fig. 5C). Further analysis of the distinct mechanical properties of taenidia fibres is shown in Fig. 6A-D. The distribution of Elastic modulus in points influenced by chitin rigidity was 0.5 to 26.5 GPa (skewness = 0.6), with a mean of 8.5 ± 8 GPa (N of trachea = 3, local indentation points = 18) (Fig. 6A). The distribution of Elastic modulus in points influenced by resilin compliance was 13.9 to 380 MPa (skewness = 0.936), with a mean of 104 \pm 96 MPa (N of trachea = 3, local indentation points = 10) (Fig. 6B). The relationship between Elastic modulus and indentation depth for rigid and compliant areas is shown in Fig. 6C-D. This variation suggests non-homogeneous material properties with a complex intrinsic organisation, associated with nano-fibre orientation, material gradient and composition.

3.4. FEM numerical results

Firstly, force-displacement curves were obtained through numerical simulations for the (i) pure resilin, and (ii) pure chitin cases described in Section 2.6. Fig. 7 shows the experimental data sets that were processed using the simulations, and the obtained numerical results. The percentage error between the experimental and numerical values was calculated using the formula

$$\varepsilon = \left| \frac{v_N - v_E}{v_F} \right| \times 100\%,$$

where ν_N is the numerical data obtained through the simulations, and ν_E is the experimental data. Both resilin related and chitin related simulations gave a percentage error around 5% (resilin: $\varepsilon=5.9\%$, chitin: $\varepsilon=4.84\%$). Hence, the numerical results matched the experimental data with high accuracy, providing validation to the mathematical models.

Once the constructed mathematical model was validated, various simulations were carried out for taenidia fibres with heterogeneous material properties as described in Section 2.6. Fig. 8 gives the Elastic modulus (E) that was calculated from applying Eq. (1) to the force-displacement curves obtained through the simulations. The Elastic modulus was sensitive to the composition of the material and ranged between 0.666 – 1.216 GPa for the considered compositions.

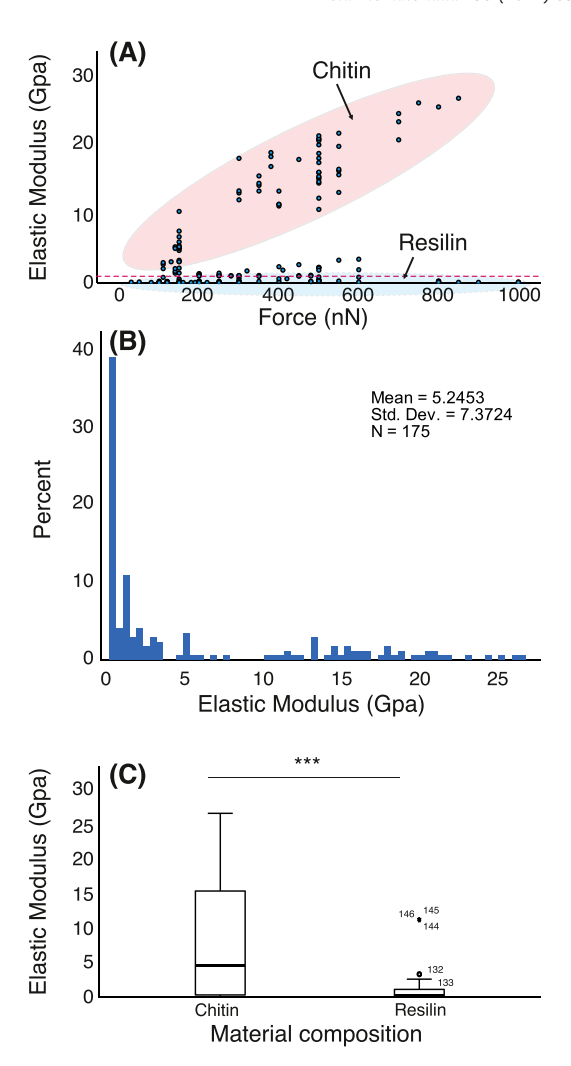


Fig. 5. Mechanical analysis of taenidia composition. (A) Variation of Elastic modulus with indentation force. (B) Histogram showing the combined mechanical characterisation of material composition (13.9 MPa to 26.5 GPa). (C) Box-and-Whisker plots showing data variation and statistical significance. The values inside the box represent the first (lower value) and third quartile, the line within the box represents the median, the (-) shows the minimum and maximum observations and the $(\circ, *)$ symbol indicates outliers. Key significance: ***, P < 0.001).

4. Discussion

We propose a new method to investigate the nanoscale mechanics of taenidia fibres in the interior surface of insects' acoustic trachea. Our approach directly accesses the reinforcement element, by isolating strips of taenidia fibres and immobilizing them into a rigid substrate. We succeeded to avoid any chemical modification that could have altered the mechanical properties of the sample. However, since the taenidia were attached on a horizontal plane, the orientation of chitin fibrils could have been affected by the lack of the in vivo cylindrical shape. Using AFM-based nanoindentation we have investigated the mechanical properties of individual taenidium of the species Mecopoda elongata at a constant velocity. Our results clearly demonstrate that taenidia fibres are composite structures, which exhibit pronounced differences in their mechanical response. This distinct mechanical behaviour is most likely associated with the mechanical properties of chitin and resilin and can be attributed to the fine point loading of the cantilever's tip. To the best of our knowledge, this is the first attempt to characterize the nanoscale structure of the tracheal tube structural elements, by considering the chitin-resilin taenidia thickenings as a single fibre.

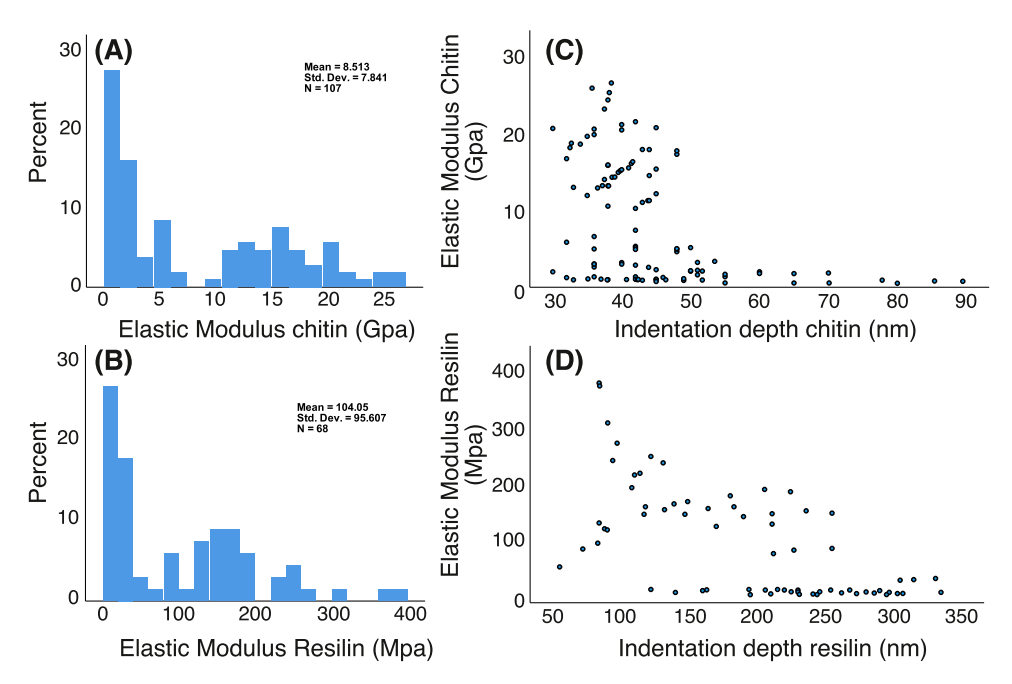


Fig. 6. Elastic response of material components and indentation depth. (A, B) Histograms of Elastic modulus distribution at local indentation points that were affected by chitin (0.5 to 26.5 GPa) and resilin (13.9 to 380 MPa). (C, D) Relation of Elastic modulus with indentation depth demonstrated the non-homogeneous material properties for each variable.

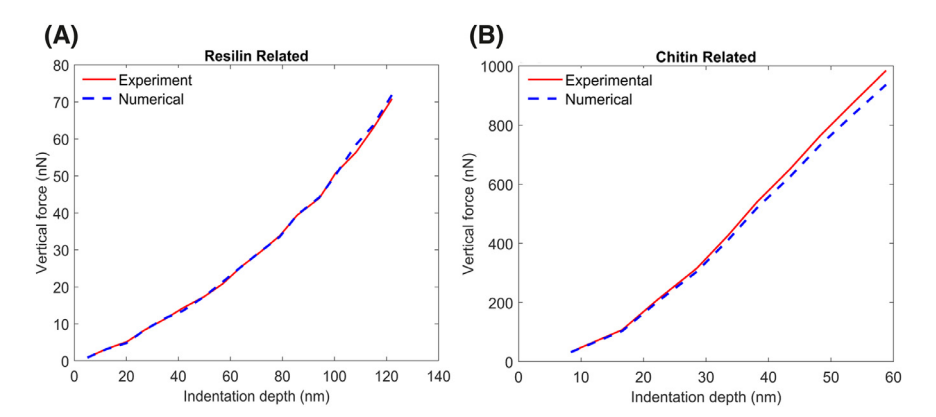


Fig. 7. Numerical simulation results using homogeneous taenidia fibre. Force-displacement curves obtained through numerical simulations and experimental measurements for (A) resilin related results, and (B) chitin related results.

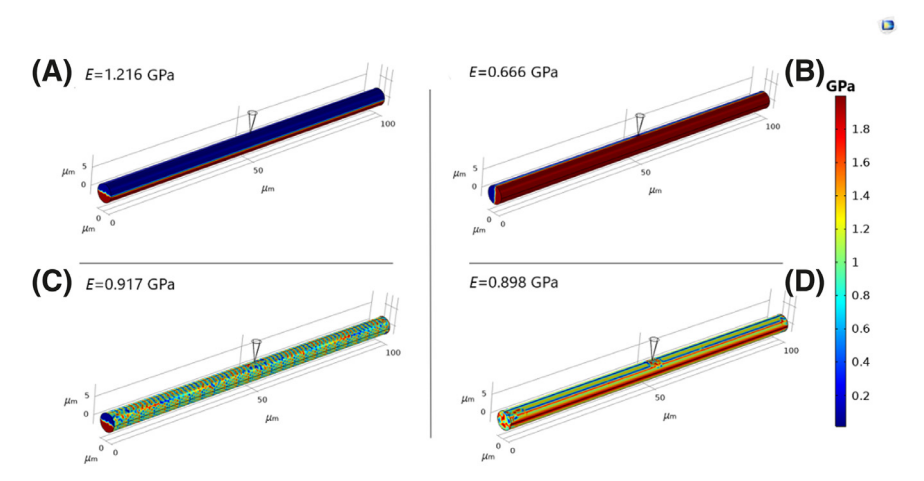


Fig. 8. Numerical simulation results using heterogeneous taenidia fibre. (A-D) The Elastic modulus (E) calculated for four taenidia fibres comprised of composite materials.

The AT is a multifunctional biological material that transmits sound and can withstand mechanical loading. While the respiratory tracheae of insects are naturally tubular in shape, and nearsymmetrical in cross section, the structure of the acoustic tracheae of Mecopoda elongata has likely been shaped by several selective evolutionary pressures related to the various stresses and strains of locomotion, and their cross-sectional symmetry has likely evolved to conform to the second moment of area (the efficiency of a shape to resist load-induced bending), which is heavily influenced by material symmetry [42]. The tube owes its mechanical rigidity to microscopic taenidia fibres, which are developed internally. The taenidia are developed as fibres that are highly aligned and densely packed. Characterization of the AT interior wall can lead to interdisciplinary research breakthroughs by facilitating advances of 3D models simulating the auditory process. In addition, accurate characterization of chitin/resilin-based cuticles in the nanoscale can inform the bottom-up development of innovative bioinspired materials.

Chitin occurs as ordered nanofibres and is the major structural component of the insect cuticle [18]. Nanofibrils of arthropods are 3 nm in diameter, a few hundred nm in length and have a high Elastic modulus (>150 GPa) [21]. Hassanzadeh et al. [43], studied the mechanics of self-assembly chitin nanofibres and derive an Elastic modulus of 5-7 GPa for single fibrils. The orientation of the chitin has a controlling influence in mechanical anisotropy and can contribute to heterogeneity of the elastic properties of the individual taenidium. From a microscopic perspective, such a reinforcement material that functions in an elliptic cylindrical shape can be assumed to be compressible. The Elastic modulus of soft cuticle ranges from kPa up to 60 MPa [27,41] and can go up to 700 MPa [46]. In the present study we used the mechanical response as a guide to facilitate categorisation of taenidia composition. Values below 400 MPa were assigned as resilin-specific and higher than 0.5 GPa as chitin-specific. Our data overall support the suggestion for a compliant material such as resilin (Fig 1C, 2C), the presence of which would improve durability and wear resistance. In combination with a rigid material, resilin would help to absorb energy caused by stresses during movement and bending, as indicated by the extended F-d retraction behaviour (Fig. 2C). The sample was fully immersed in saline and was kept well hydrated during all experiments. It has been suggested that water content is important in the resulting mechanical parameters of the cuticle. A 5% reduction in water can result in a 10-fold increase in Elastic modulus [28,44]. During sample preparation, the maximum time that the sample was kept out of aqueous media was less than 2 minutes. Since resilin is maintained well hydrated in its natural state [28], this experimental procedure ensured preservation of the elastic properties of the sample. However, since the AT is filled with air, the Elastic modulus in vivo may be higher than the values measured in this study, using hydrated samples.

The Hertz model is commonly used to extract the Elastic modulus of biological materials from a force-displacement curve acquired by indentation measurements [29,45,46]. Considering heterogeneity and inherent complexity of biological materials, a sharp tip may lead to significant differences between measurements due to small tip-sample contact area [47]. To avoid complications in the interpretation of the data using the Hertz model the depth of indentation was much smaller than the thickness of the sample. In addition to composition, the increased heterogeneity of the results (MPa to GPa) may be attributed to the sharp tip indentation, which is able to produce nanoscale deformations between chitin fibrils adding substantially to modulus variation. It is possible that mechanical properties can change substantially even across the surface of single taenidium. Our data demonstrate that it is important to perform triplicate F-d measurements with incremental

forces at each local point. There are inevitable forces applied to the sample during preparation that may alter the nanoscale structure of the taenidia, such as tensile forces applied during the attachment of the microsample to the substrate. However, we expect that only the softer cuticle in the space between the taenidia near the points of attachment would have been affected. Taenidia fibres in the middle of the microsample would be less susceptible and were chosen for testing. Overall, the distribution of modulus is greater than the uncertainty of the experimental technique and can be explained by differences in composition of the fibres [48]. We have not identified specific differences of mechanical properties based on the section of the trachea (proximal to distal) from which the taenidia sample was extracted. All microstrips were extracted by the forefemur where the tube is uniform in diameter.

Overall, our results are in the expected range of insect cuticle materials ranging from hundreds of MPa to GPa [11,28,49] as reported in the literature, including the elasticity of tracheal tubes measured in other insects [12,27,50], and are strongly affected by the composition of the tube. Peisker et al. [11,49], identified a gradient in cuticle elasticity of the beetle *Coccinella septempunctata*, which was position and resilin dependent ranging from 1.2 MPa to 6.8 GPa. It was also evident that the resilin content had a significant role in the elastic recovery of the material, a phenomenon that was also present in our study.

The heterogeneity between local indentation points of the taenidia was further supported by the numerical results. For the numerical simulations, both homogeneous and heterogeneous cases of the taenidium were considered. Once the mathematical models were validated through a comparison with experimental data for the homogeneous resilin and chitin cases (Fig. 7), four different compositions of the material were also considered (see Fig. 8). The Elastic modulus obtained from the composite material simulations were observed to be sensitive not only to the percentage of resilin and chitin present in the material, but also to the location of these structures. For instance, the compositions given in Fig. 8A and Fig. 8B both have 50% resilin and 50% chitin. Nevertheless, we obtained a significant difference in the calculated Elastic moduli (1.216 GPa in Fig. 8A and 0.666 GPa in Fig. 8B). Numerical results further suggested that different compositions along the surface also have a significant effect on the Elastic modulus. As can be observed in Fig. 8A and Fig. 8C, the material composition inside of the taenidia fibre is the same in both cases, however, in the case shown at Fig. 8C we have arbitrarily varied the composition of the surface. This ended up changing the measured Elastic modulus from 1.216 GPa to 0.917 GPa. Finally, considering the composition as strands of resilin and chitin as shown in Fig. 8D, led to another distinct Elastic modulus, where it was calculated as 0.898 GPa. Hence, the numerical results demonstrate the sensitivity of the results to the composition of the material. These results also suggest that the wide range of results obtained from experimentation for the Elastic modulus is due to the complex composite structure of the taenidia fibre.

Numerical simulations were also used to check the effect of the taenidia dimensions on the results. Changes in the length (50-400 $\mu m)$ or the radius (1.5-5 $\mu m)$ of the fibre did not, however, lead to a significant change in the reaction force. Furthermore, to test the influence of the surface curvature, the cylindrical shape used for the taenidia was replaced by a block in the simulations. Hence, in this case the surface of the fibre was completely flat. This did not lead to any significant differences in the results either, strongly suggesting that due to the small size of the indenter tip (radius 10 nm), the fibre dimensions and curvature of the contact surface do not have a significant influence on the reaction force.

5. Conclusion

Nanomechanical characterisation of insect cuticle is a challenging interdisciplinary task [50], and measurements of the Elastic modulus varied considerably in our study. Nanoindentation curves captured pronounced differences in the mechanical response of taenidia that were extracted from acoustic tracheae of the bushcricket Mecopoda elongata (13.9 MPa to 26.5 GPa). We suggest that the modulus variation is due to complex material composition, comprised of smaller fibrils of chitin, resilin protein, and the fine characteristics of the indenter tip (<10 nm). At indentation depths up to 400 nm, we were able to capture the differences in the mechanical response of the chitin-resilin interplay and analyse their complex nanoscale deformation behaviour. Mechanical analysis facilitated classification of data to chitin-resilin-related categories. Values of Elastic modulus lower than 380 MPa were associated with soft resilin, which comprised 38% of the full data set. Our results overall suggest that taenidia fibres are complex micromechanical elements, whose composition and fundamental mechanics have been adapted to optimise function under various stresses and strains during locomotion.

Funding

This work was supported by the European Research Council [ERCCoG-2017-773067, 2017 to F.M.-Z.], The Natural Environment Research Council [DEB-1937815, 2019 to FM-Z] The AFM-FS was supported by an equipment grant from Diabetes UK [12/0004546, 2012 to PS].

Declaration of Competing Interest

The authors declare that they have no known competing financial interests or personal relationships that could have appeared to influence the work reported in this paper.

Acknowledgement

We thank Prof. Malcolm Burrows at the University of Cambridge for the kind use of his resilin imaging microscope and camera. We also thank Dr Karin Muller at the Cambridge Advance Imaging Centre for her support using the Scanning Electron Microscope.

Supplementary materials

Supplementary material associated with this article can be found, in the online version, at doi:10.1016/j.actbio.2022.08.056.

References

- F. Montealegre-Z, T. Jonsson, K.A. Robson-Brown, M. Postles, D. Robert, Convergent evolution between insect and mammalian audition, Science 338 (6109) (2012) 968–971.
- [2] W.J. Bailey, The tettigoniid (orthoptera, tettigoniidae) ear multiple functions and structural diversity, Int. J. Insect Morphol. Embryol. 22 (2-4) (1993) 185–205.
- [3] R. Heinrich, M. Jatho, K. Kalmring, Acoustic transmission characteristics of the tympanal tracheas of bush-crickets (Tettigoniidae) .2. Comparative-studies of the tracheas of 7 species, J. Acoust. Soc. Am. 93 (6) (1993) 3481–3489.
- [4] J.X. Shen, A peripheral mechanism for auditory directionality in the bush-cricket *Gampsocleis gratiosa*: acoustic tracheal system, J. Acoust. Soc. Am. 94 (3) (1993) 1211–1217.
- [5] A. Michelsen, K.G. Heller, A. Stumpner, K. Rohrseitz, A new biophysical method to determine the gain of the acoustic trachea in bush-crickets, J. Comp. Physiol. A Sens. Neural Behav. Physiol. 175 (2) (1994) 145–151.
- [6] M. Nowotny, J. Hummel, M. Weber, D. Moeckel, M. Koessl, Acoustic-induced motion of the bushcricket (Mecopoda elongata, Tettigoniidae) tympanum, J. Comp. Physiol. A Sens. Neural Behav. Physiol. 196 (12) (2010) 939–945.

- [7] D. Veitch, E. Celiker, S. Aldridge, C. Pulver, C. Soulsbury, T. Jonsson, C. Woodrow, F. Montealegre-Z, A narrow ear canal reduces sound velocity to create additional acoustic inputs in a micro-scale insect ear, Proc. Natl. Acad. Sci. 118 (10) (2020) e2017281118.
- [8] K. Kalmring, W. Rossler, R. Ebendt, J. Ahi, R. Lakes, The auditory receptor organs in the forelegs of bush-crickets physiology, receptor cell arrangement, and morphology of the tympanal and intermediate organs of 3 closely related species, Zool. Jahrb., Abt. Allg. Zool. Physiol. Tiere 97 (1) (1993) 75–94.
- [9] J. Hummel, M. Kössl, M. Nowotny, Morphological basis for a tonotopic design of an insect ear, J. Comp. Neurol. 525 (10) (2017) 2443–2455.
- [10] H. Stolting, A. Stumpner, Tonotopic organization of auditory receptors of the bushcricket Pholidoptera griseoaptera (Tettigoniidae, Decticinae), Cell Tissue Res. 294 (2) (1998) 377–386.
- [11] H. Peisker, J. Michels, S.N. Gorb, Evidence for a material gradient in the adhesive tarsal setae of the ladybird beetle Coccinella septempunctata, Nat. Commun. 4 (1) (2013) 1–7.
- [12] M.R. Webster, R. De Vita, J.N. Twigg, J.J. Socha, Mechanical properties of tracheal tubes in the American cockroach (Periplaneta americana, Smart Mater. Struct. 20 (9) (2011) 094017.
- [13] M. Jafarpour, S. Eshghi, A. Darvizeh, S. Gorb, H. Rajabi, Functional significance of graded properties of insect cuticle supported by an evolutionary analysis, J. Royal Soc. Interface 17 (168) (2020) 20200378.
- [14] N. Barbakadze, S. Enders, S. Gorb, E. Arzt, Local mechanical properties of the head articulation cuticle in the beetle Pachnoda marginata (Coleoptera, Scarabaeidae), J. Exp. Biol. 209 (4) (2006) 722–730.
- [15] H. Rajabi, M. Jafarpour, A. Darvizeh, J.-H. Dirks, S. Gorb, Stiffness distribution in insect cuticle: a continuous or a discontinuous profile? J. Royal Soc. Interface 14 (132) (2017) 20170310.
- [16] M.J. Klowden, Physiological Systems in Insects, Elsevier Inc., 2008 Second Edition ed
- [17] K. Dittrich, B. Wipfler, A review of the hexapod tracheal system with a focus on the apterygote groups, Arthropod Struct. Develop. 63 (2021) 101072.
- [18] R.F. Chapman, The Insects: Structure and Function, Cambridge University Press, Cornell University, New York, 2013.
- [19] J.M. Whitten, Comparative anatomy of the tracheal system, Annu. Rev. Entomol. 17 (1) (1972) 373–402.
- [20] V.B. Wigglesworth, The properties of the lining membrane of the insect tracheal system, Tissue Cell 22 (2) (1990) 231–238.
- [21] J.F. Vincent, Arthropod cuticle: a natural composite shell system, Composites, Part A 33 (10) (2002) 1311–1315.
- [22] M.W. Westneat, O. Betz, R.W. Blob, K. Fezzaa, W.J. Cooper, W.-K. Lee, Tracheal respiration in insects visualized with synchrotron X-ray imaging, Science 299 (5606) (2003) 558–560.
- [23] R. Balu, N.K. Dutta, A.K. Dutta, N.R. Choudhury, Resilin-mimetics as a smart biomaterial platform for biomedical applications, Nat. Commun. 12 (1) (2021)
- [24] G. Qin, X. Hu, P. Cebe, D.L. Kaplan, Mechanism of resilin elasticity, Nat. Commun. 3 (1) (2012) 1–9.
- [25] R.S.-C. Su, Y. Kim, J.C. Liu, Resilin: protein-based elastomeric biomaterials, Acta Biomater. 10 (4) (2014) 1601–1611.
- [26] P.-Y. Chen, J. McKittrick, M.A. Meyers, Biological materials: Functional adaptations and bioinspired designs, Prog. Mater Sci. 57 (8) (2012) 1492–1704.
- [27] M.R. Webster, J.J. Socha, L. Teresi, P. Nardinocchi, R. De Vita, Structure of tracheae and the functional implications for collapse in the American cockroach, Bioinspiration Biomimetics 10 (6) (2015) 066011.
- [28] J.F.V. Vincent, U.G.K. Wegst, Design and mechanical properties of insect cuticle, Arthropod Struct. Dev. 33 (3) (2004) 187–199.
- [29] E. Siamantouras, C.E. Hills, P.E. Squires, K.-K. Liu, Quantifying cellular mechanics and adhesion in renal tubular injury using single cell force spectroscopy, Nanomed. Nanotechnol. Biol. Med. 12 (4) (2016) 1013–1021.
- [30] E. Celiker, T. Jonsson, F. Montealegre-Z, The auditory mechanics of the outer ear of the bush cricket: a numerical approach, Biophys. J. 118 (2) (2020) 464–475.
- [31] T. Jonsson, F. Montealegre-Z, C.D. Soulsbury, K.A. Robson Brown, D. Robert, Auditory mechanics in a bush-cricket: direct evidence of dual sound inputs in the pressure difference receiver, J. Royal Soc. Interface 13 (122) (2016).
- [32] I.N. Sneddon, The relation between load and penetration in the axisymmetric Boussinesq problem for a punch of arbitrary profile, Int. J. Eng. Sci. 3 (1) (1965) 47–57.
- [33] V.M. Laurent, S. Kasas, A. Yersin, T.E. Schäffer, S. Catsicas, G. Dietler, A.B. Verkhovsky, J.-J. Meister, Gradient of rigidity in the lamellipodia of migrating cells revealed by atomic force microscopy, Biophys. J. 89 (1) (2005) 667-675.
- [34] M. Radmacher, M. Fritz, C.M. Kacher, J.P. Cleveland, P.K. Hansma, Measuring the Viscoelastic Properties of Human Platelets with the Atomic Force Microscope, Elsevier, 1996.
- [35] J.E. Sader, J.W.M. Chon, P. Mulvaney, Calibration of rectangular atomic force microscope cantilevers, Rev. Sci. Instrum. 70 (10) (1999) 3967–3969.
- [36] E.K. Dimitriadis, F. Horkay, J. Maresca, B. Kachar, R.S. Chadwick, Determination of elastic moduli of thin layers of soft material using the atomic force microscope, Biophys. J. 82 (5) (2002) 2798–2810.
- [37] H.-J. Butt, M. Jaschke, Calculation of thermal noise in atomic force microscopy, Nanotechnology 6 (1) (1995) 1.
- [38] J.L. Hutter, J. Bechhoefer, Calibration of atomic-force microscope tips, Rev. Sci. Instrum. 64 (7) (1993) 1868–1873.

- [39] E. Holzbecher, H. Si, Accuracy tests for COMSOL-and Delaunay meshes, in: Proceedings of the COMSOL Conference, 2008, p. 7.
- [40] Comsol Multiphysics. Structural Mechanics Module, User's Guide, Stokolm, Sweden, 2020.
- [41] M. Burrows, Development and deposition of resilin in energy stores for locust jumping, J. Exp. Biol. 219 (16) (2016) 2449–2457.

 [42] S.A. Wainwright, J. Gosline, W. Biggs, J.D. Currey, Mechanical Design in Organ-
- isms, Princeton University Press, 1982.
- [43] P. Hassanzadeh, W. Sun, J.P. de Silva, J. Jin, K. Makhnejia, G.L. Cross, M. Rolandi, Mechanical properties of self-assembled chitin nanofiber networks, J. Mater. Chem. B 2 (17) (2014) 2461–2466.
- [44] S.E. Reynolds, The mechanical properties of the abdominal cuticle of Rhodnius larvae, J. Exp. Biol. 62 (1) (1975) 68–80.
- [45] S. Kasas, G. Longo, G. Dietler, Mechanical properties of biological specimens explored by atomic force microscopy, J. Phys. D Appl. Phys. 46 (13) (2013)
- [46] E. Siamantouras, C.E. Hills, M.Y. Younis, P.E. Squires, K.-K. Liu, Quantitative investigation of calcimimetic R568 on beta cell adhesion and mechanics using AFM single-cell force spectroscopy, FEBS Lett. 588 (7) (2014) 1178–1183.
- [47] L. Qian, H. Zhao, Nanoindentation of soft biological materials, Micromachines 9 (12) (2018) 654.
- [48] P. Dutov, O. Antipova, S. Varma, J.P. Orgel, J.D. Schieber, Measurement of elastic modulus of collagen type I single fiber, PLoS One 11 (1) (2016) e0145711.
- [49] D. Klocke, H. Schmitz, Water as a major modulator of the mechanical properties of insect cuticle, Acta Biomater. 7 (7) (2011) 2935–2942.
 [50] K. Stamm, B.D. Saltin, J.-H. Dirks, Biomechanics of insect cuticle: an interdisci-
- plinary experimental challenge, Appl. Phys. A 127 (5) (2021) 329.